

# Individualized fMRI-targeted rTMS for neuropsychiatric sequelae of repetitive head trauma in a retired NFL player

Shan H. Siddiqi, Nicholas T. Trapp, Carl D. Hacker, Timothy O. Laumann, Sridhar Kandala, Pashtun Shahim, Alexandre R. Carter, David L. Brody

---

## **Supplementary Information**

### **1. MRI acquisition and pre-processing**

1.1: Acquisition .....	2
1.2: BOLD Pre-processing.....	2
Figure S1: Baseline anatomical MRI.....	3
Figure S2: BOLD quality control parameters.....	4-5

### **2. Functional connectivity analysis**

2.1: Seed-based connectivity analysis.....	6
Table S1: List of regions of interest (ROIs) used for seed-based analysis.....	6
Figure S3: Regions used as seed ROIs based on group-mean studies .....	6
2.2: Cortical parcellation .....	7
Figure S4: Winner-take-all map of individualized network boundaries .....	7
Figure S5: Seed-based correlations for subject (pre/post rTMS) and comparators .....	8
Figure S6: Whole-brain stimulation site connectivity before and after treatment .....	9

Supplementary references.....	10
-------------------------------	----

## 1. MRI acquisition and pre-processing

### 1.1 Acquisition

Functional and anatomical images were acquired with a 3T Siemens Magnetom Prisma magnetic resonance scanner (Siemens, Erlangen, Germany). Acquisition included 16.5 minutes of resting-state blood oxygen-level dependent (BOLD) scans in three runs (416 frames per run, 48 axial slices using 4-band acquisition, 3 mm cubic voxel resolution, repetition time (TR) 800 ms, echo time (TE) 26.6 ms, flip angle 61 degrees, imaging matrix 72 x 72) in addition to a T1 MPRAGE structural sequence (176 frames, 0.9375 x 0.9375 x 1 mm voxel resolution, TR 2400 ms, TE 3.19 ms, flip angle 8 degrees, imaging matrix 256 x 256).

### 1.2 BOLD Pre-processing

Spatial alignment and atlas/native space transformations were performed using the 4dfp suite of tools developed at Washington University. Anatomical segmentation and surface reconstruction was conducted using Freesurfer (version 5.3.0, Human Connectome Project release)[1] on the subject's T1-weighted anatomical MRI scan (figure S1). Motion censoring with framewise displacement (FD) of 0.5 mm, nuisance regression, global signal regression, temporal filtering, spatial smoothing, and motion epoch interpolation were performed using in-house scripts described in Power et al., 2014 [2].

The resulting quality control plots (figure S2) for the pre-treatment and post-treatment scans were used to estimate the influence of artifact from head motion and nuisance signals via the qualitative approach described in Power, 2016[3]. These plots were used to calculate frame-wise FD (framewise displacement of the head after realignment) and DVARS (root mean square value of the overall change in signal intensity between frames). The Pearson correlation between FD and DVARS was calculated in order to determine the influence of head motion on overall BOLD signal fluctuations; reductions in this value are often used to estimate the degree to which motion-related signal fluctuations were corrected by processing[4]. After processing, FD-DVARS correlation was reduced both for pre-treatment scans (from  $r = 0.63$  to  $r = 0.08$ , 459/1248 frames retained) and post-treatment scans (from  $r = 0.69$  to  $r = 0.13$ , 626/1248 frames retained).

The original FD threshold of 0.5 mm was chosen because the noise floor of the FD values were substantially higher than what is typically reported. In order to retain enough post-censoring data to permit network mapping and treatment targeting, we followed the less conservative FD threshold recommended in Power et al., 2012[5] which is now widely used in the field. While the recommendation was revised to 0.2 mm in Power et al., 2014, this paper also specified that the optimal parameters would require adjustment due to the capabilities of newer scanners, including faster TR, multi-band acquisitions, and improved signal-to-noise ratio[2]. For our subject, the ability to form reliable resting-state network maps[6] for treatment targeting (which is reliant on the quantity of available BOLD data and was initially validated[6] using the Power 2012 censoring parameters[5]) was prioritized over the ability to reliably remove distance-dependent artifact in post-treatment functional connectivity analyses (which is heavily dependent on FD threshold).

Furthermore, it has previously been observed that motion parameters derived from fast TR data (less than 1 second, as in this study) often contain high frequency factitious movement associated with respiration that will artifactually increase measured FD values[2,7]. This issue may be exaggerated here due to the subject's relatively large stature[7]. To investigate the impact of the FD threshold on reduction of motion-related BOLD signal fluctuations, processing was repeated with a more aggressive FD threshold of 0.3 mm, which yielded similar pre- and post-treatment values of  $r = 0.06$  (212/1248 frames retained) and  $r = 0.02$  (296/1248 frames retained), respectively. Fast Fourier Transform of the FD trace revealed peaks in the power spectrum in the range of 0.35-0.40 Hz, which is consistent with respiratory motion; the full analysis was thus repeated using a 0.35 Hz low-pass filter on the FD trace in order to correct for respiratory motion as described by Siegel et al., 2016[7]. The data were subsequently re-processed with FD of 0.2 mm, which led to increased frame retention (758/1248 in pre-treatment scans and 501/1248 in post-treatment scans)but did not materially change the resting-state correlations calculated from the processed data. On average, the difference between correlation values from this analysis and the original analysis was 0.02 (SD 0.08) for the values reported in figures 4 and S5.

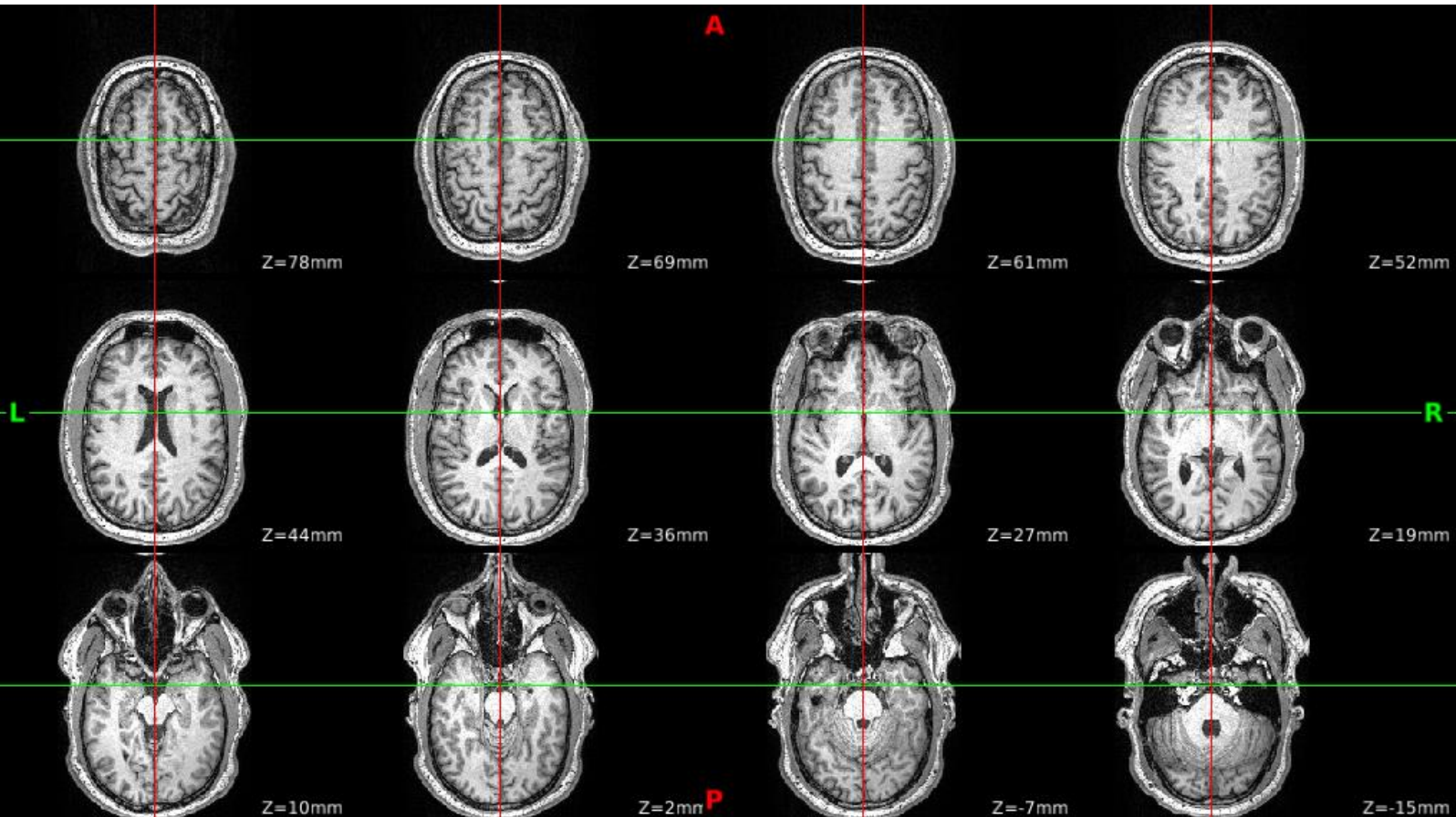


**Figure S1** Axial view of subject's T1-weighted anatomical MRI scan. No gross abnormalities were noted. Reference alignment lines are added for the purpose of comparing slices to one another; red and green reference lines represent the center of the image along the x- and y-axes, respectively.

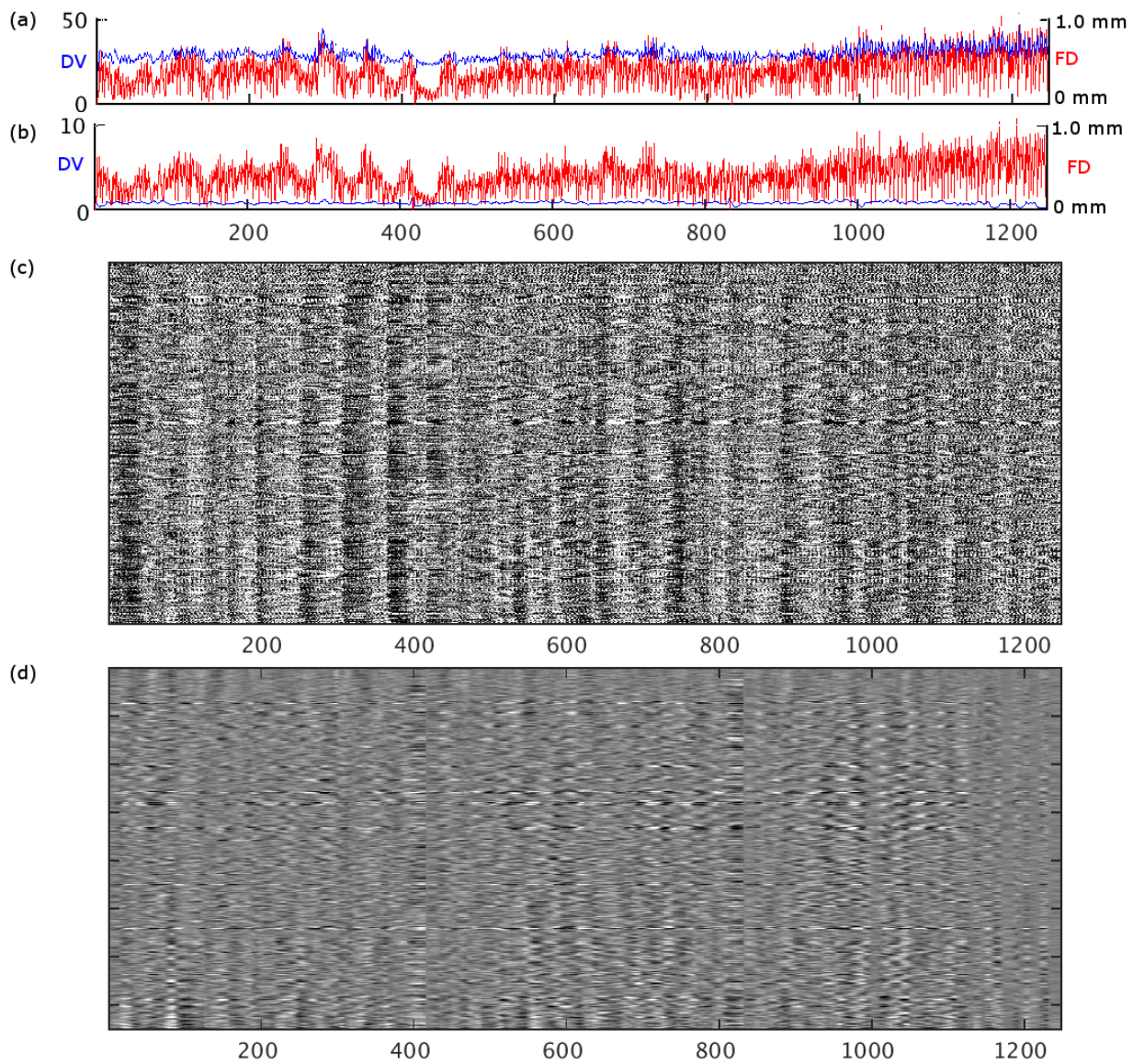
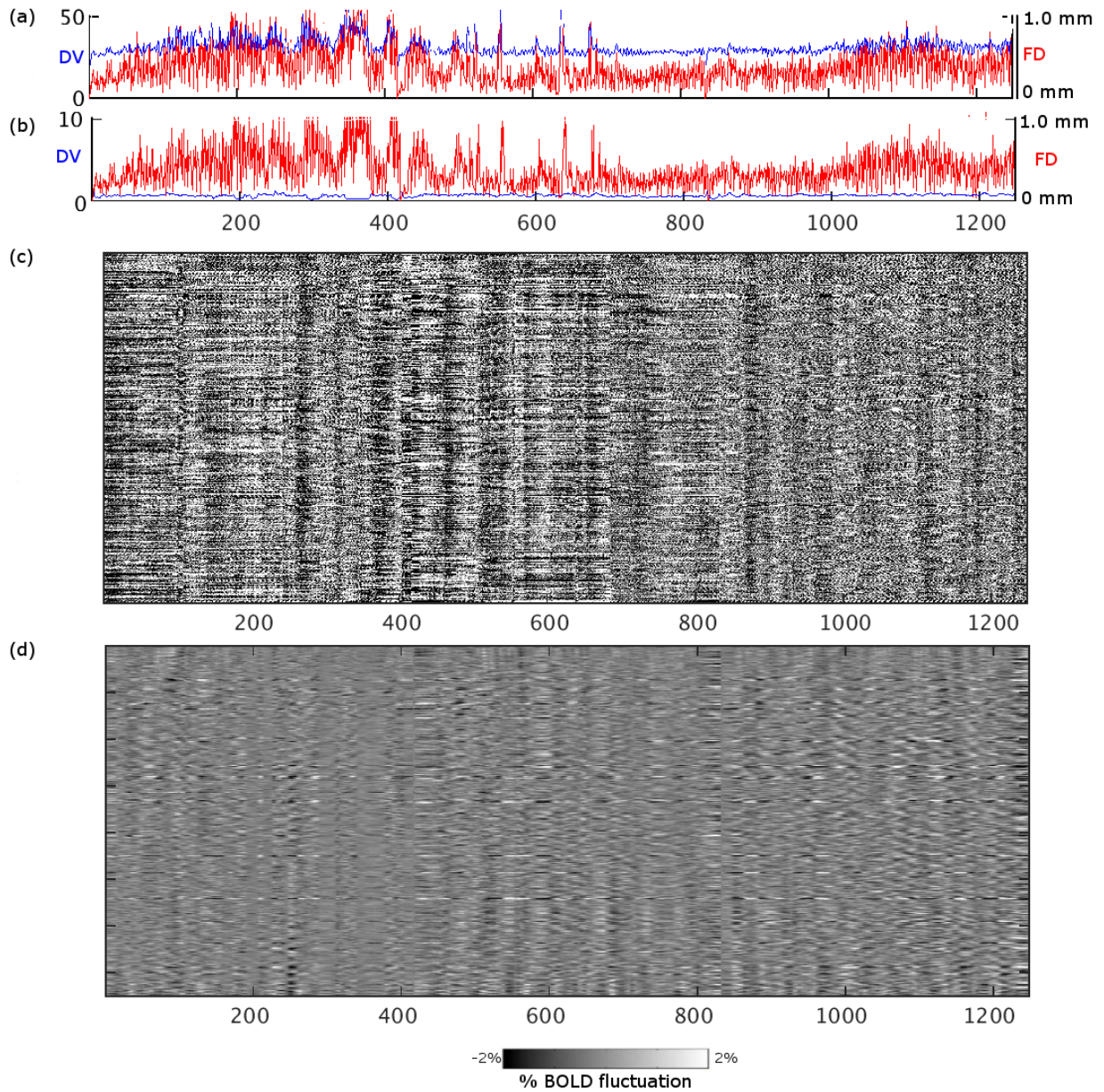


Figure S2 (continued on next page)



**Figure S2** Quality control plots[3] for full timecourse extracted from rsfMRI sequence before (top) and after (bottom) rTMS treatment course. For each plot, the x-axis represents the frame number across the timecourse (1248 total frames in each scan). Motion parameters showed reduction of DV (framewise BOLD signal fluctuation) and dissociation between DV and FD (framewise displacement) between pre-processing (a) and post-processing (b) plots for each scan. Voxel-wise BOLD signal fluctuations were also reduced between pre-processing (c) and post-processing (d) plots for each scan; the y-axis for these plots represents the total framewise BOLD fluctuation for each of the 147,456 voxels in the image.

## 2. Functional connectivity analysis

### 2.1 Seed-based connectivity analysis

BOLD timecourses were analyzed for seed-based functional connectivity by determining correlation matrices between several regions of interest (ROIs), including both individualized parcels and group-mean parcels (table S1). The absolute differences in Fisher-transformed ROI-ROI correlations were compared between pre-treatment scans, post-treatment scans, and control subjects. Seed-based correlation maps for the left- and right-sided rTMS targets were generated for the experimental subject's pre-treatment and post-treatment scans.

Region of interest	Identification method
Dorsal attention network (DAN)	Subject-specific winner-take-all map (figure S4)
Ventral attention network (VAN)	Subject-specific winner-take-all map (figure S4)
Default mode network (DMN)	Subject-specific winner-take-all map (figure S4)
Medial orbitofrontal cortex (mOFC)	Medial half of parcel 10 defined by Yeo et al., 2011 (figure S3) [14]
Lateral orbitofrontal cortex (lOFC)	Lateral half of parcel 10 defined by Yeo et al., 2011 (figure S3) [14]
Medial temporal lobe (MTL)	Parcel 9 defined by Yeo et al., 2011 (figure S3) [14]
Left/right sgACC	10-mm sphere at coordinates defined by Fox et al., 2012 (figure S3) [8]
Left/right nucleus accumbens (NAcc)	6-mm sphere at coordinates defined in Talairach Daemon atlas (figure S3) [15]
Left/right rTMS target	15-mm sphere at coordinates generated by TMS targeting algorithm (figure 1)

**Table S1** ROIs used for seed-based correlation analysis

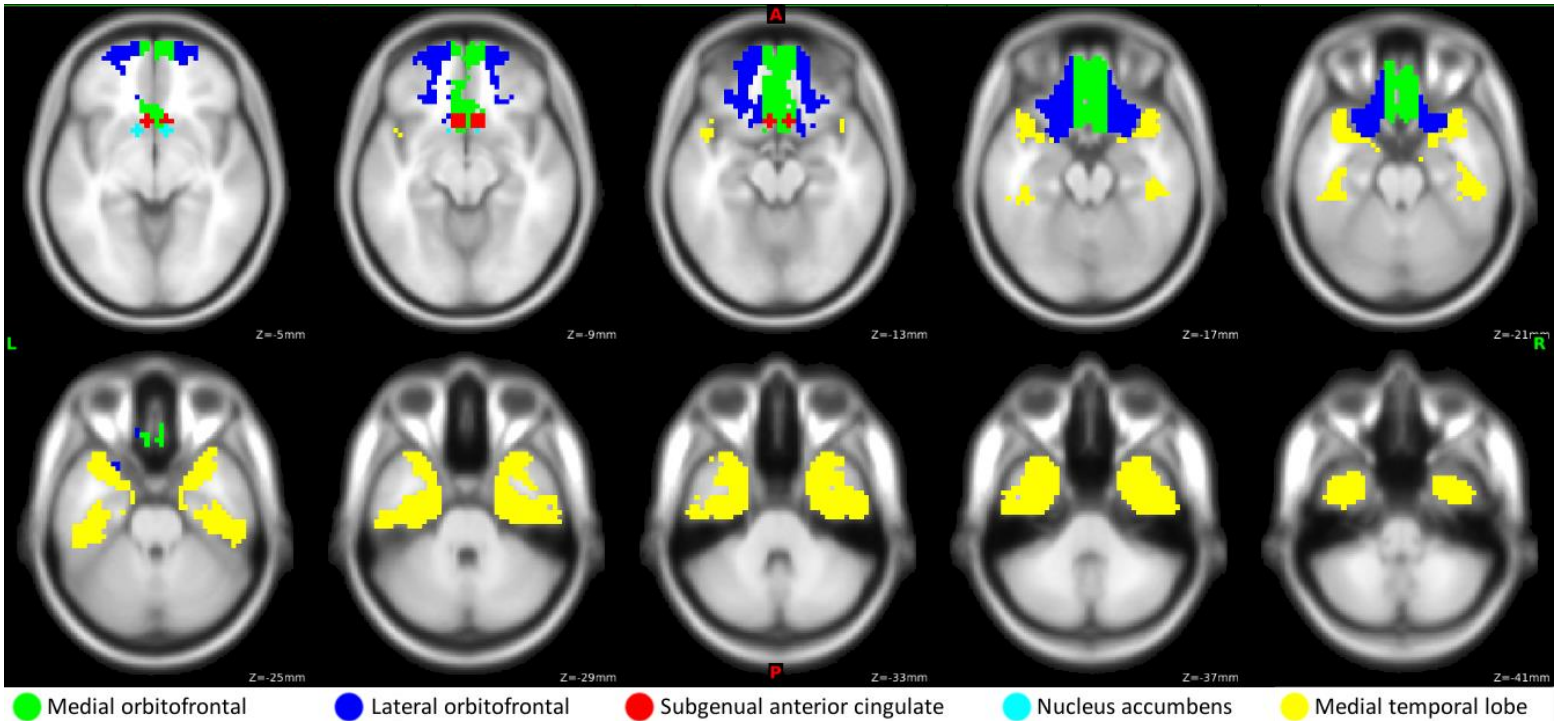


**Figure S3** Group-based ROIs used for seed-based connectivity analysis with medial/lateral orbitofrontal cortex, subgenual anterior cingulate cortex, and nucleus accumbens.

## 2.2 Cortical parcellation

For both the subject and a representative healthy control, baseline individual-level parcellation revealed inter-individual variability in location, size, and left-right symmetry of dorsal attention, ventral attention, frontoparietal, and default mode networks, particularly in the prefrontal cortex (figure S4). Due to this spatial variability, these individual subject parcels were used for ROI-based connectivity analysis in order to achieve greater individualized precision than what is possible with group-mean parcellations.

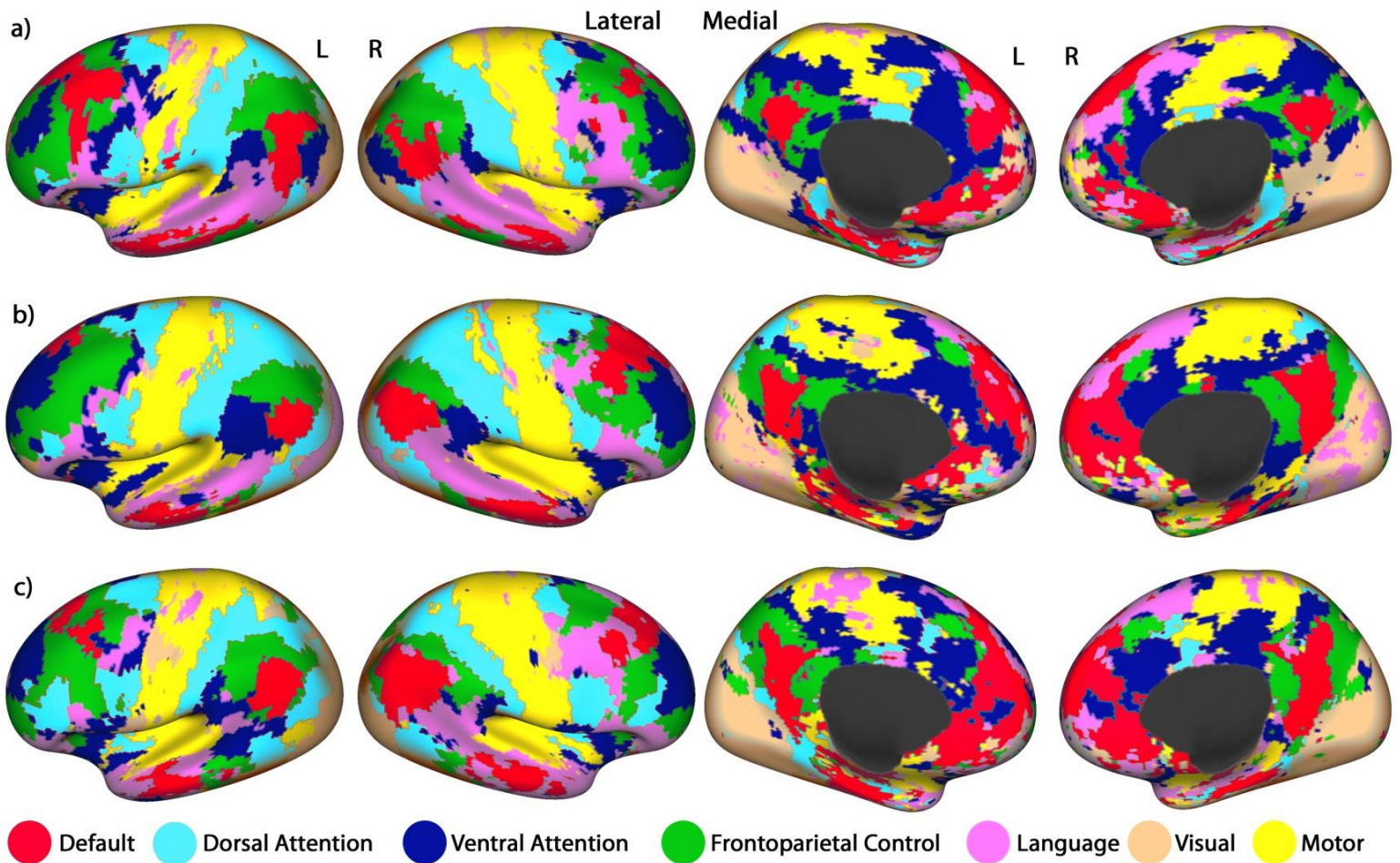


**Figure S4 Winner-take-all maps of individualized resting-state network boundaries** for (a) the experimental subject, (b) group mean of healthy comparators, and (c) a representative example of a healthy comparator. For visualization, maps are projected onto a mean inflated surface from the Human Connectome Project – this schematic representation is used rather than the subject’s own brain in order to clearly visualize between-subject differences. The subject’s individualized default, dorsal attention, and ventral attention parcels (a) were utilized for seed-based connectivity analysis.

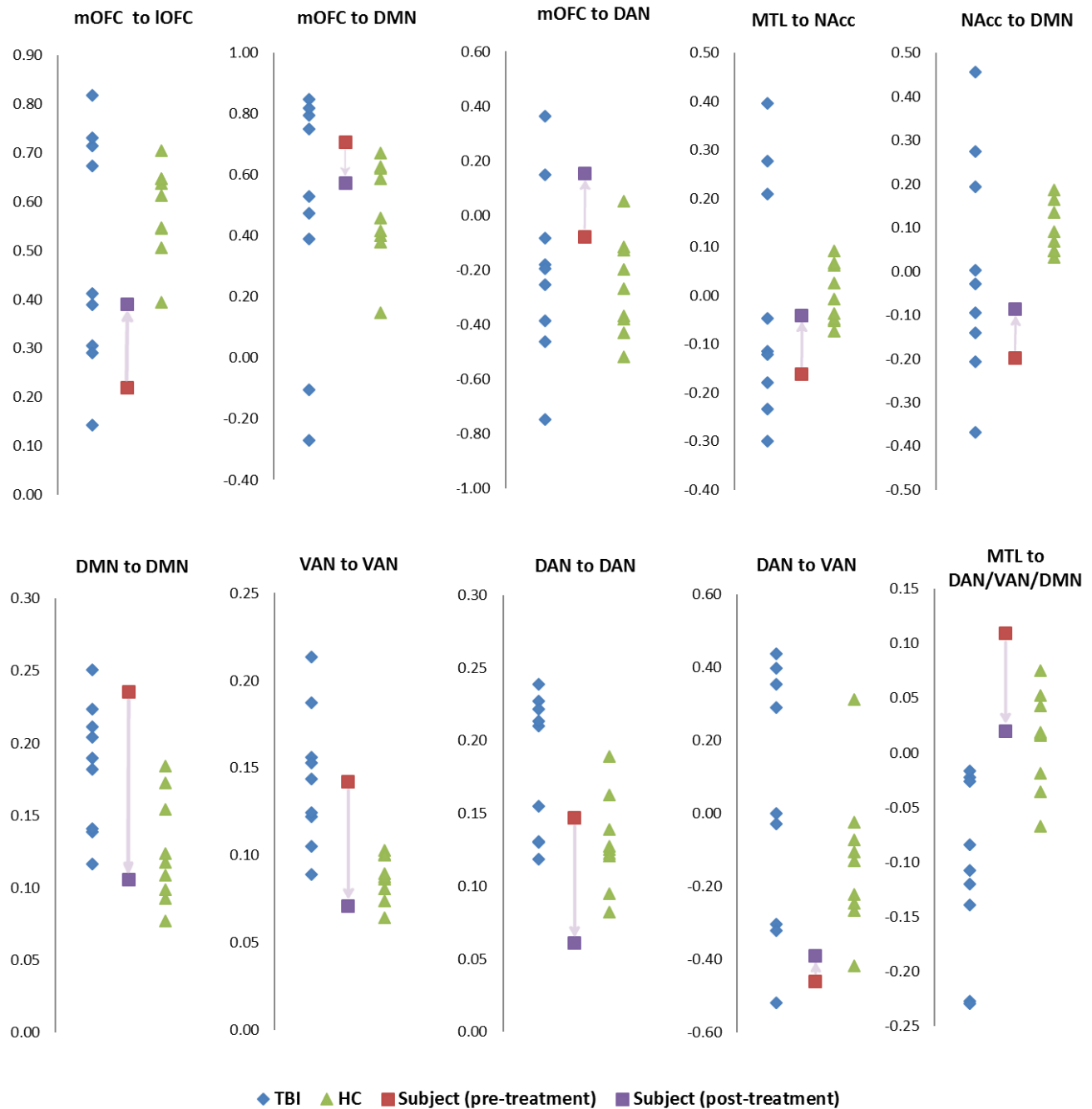


**Figure S5** Baseline seed-based connectivity analysis revealed several correlations that were outside the range of healthy controls. Some correlations (MTL to DMN, MTL to DAN/VAN/DMN, and DAN to DMN) were also outside the range of comparator subjects with TBI-associated depression. MTL to DMN and MTL to DAN/VAN/DMN correlations were higher than both comparator groups and decreased with treatment. DAN to DMN connectivity was also higher than both comparator groups, but increased further with treatment. Voxel-wise DAN to DAN connectivity was within the normal range before treatment, but became lower than all subjects after treatment.

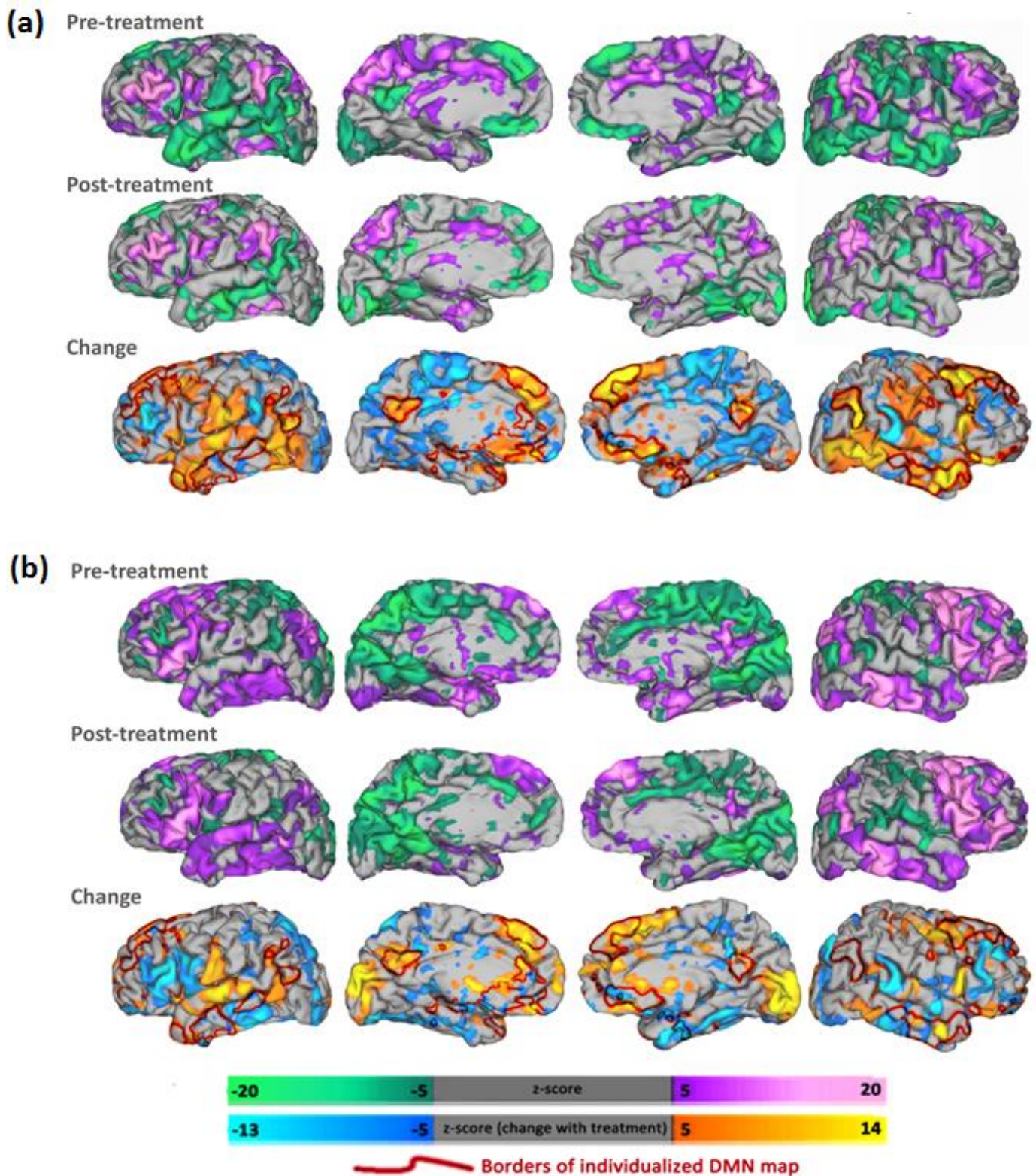


**Figure S6 Whole-brain connectivity before and after treatment. (a)** Seed-based correlation with a 15-mm spherical ROI at the left-sided rTMS target, including pre-treatment map (top), post-treatment map (middle), and change with treatment (bottom) depicted along with individualized DMN borders (red lines). **(b)** Seed-based correlation with right-sided rTMS target, including pre-treatment map (top), post-treatment map (middle), and change with treatment (bottom) depicted along with individualized DMN borders (red).

## SUPPLEMENTARY REFERENCES

- [1] Reuter M, Schmansky NJ, Rosas HD, Fischl B. Within-subject template estimation for unbiased longitudinal image analysis. *Neuroimage* 2012;61:1402–18. doi:10.1016/j.neuroimage.2012.02.084.
- [2] Power JD, Mitra A, Laumann TO, Snyder AZ, Schlaggar BL, Petersen SE. Methods to detect, characterize, and remove motion artifact in resting state fMRI. *Neuroimage* 2014;84:320–41. doi:10.1016/j.neuroimage.2013.08.048.
- [3] Power JD. A simple but useful way to assess fMRI scan qualities. *Neuroimage* 2016. doi:10.1016/j.neuroimage.2016.08.009.
- [4] Muschelli J, Nebel MB, Caffo BS, Barber AD, Pekar JJ, Mostofsky SH. Reduction of motion-related artifacts in resting state fMRI using aCompCor. *Neuroimage* 2014;96:22–35. doi:10.1016/j.neuroimage.2014.03.028.
- [5] Power JD, Barnes KA, Snyder AZ, Schlaggar BL, Petersen SE. Spurious but systematic correlations in functional connectivity MRI networks arise from subject motion. *Neuroimage* 2012;59:2142–54. doi:10.1016/j.neuroimage.2011.10.018.
- [6] Hacker CD, Laumann TO, Szrama NP, Baldassarre A, Snyder AZ, Leuthardt EC, et al. Resting state network estimation in individual subjects. *Neuroimage* 2013;82:616–33. doi:10.1016/j.neuroimage.2013.05.108.
- [7] Siegel JS, Mitra A, Laumann TO, Seitzman BA, Raichle M, Corbetta M, et al. Data Quality Influences Observed Links Between Functional Connectivity and Behavior. *Cereb Cortex* 2016. doi:10.1093/cercor/bhw253.
- [8] Fox MD, Buckner RL, White MP, Greicius MD, Pascual-Leone A. Efficacy of transcranial magnetic stimulation targets for depression is related to intrinsic functional connectivity with the subgenual cingulate. *Biol Psychiatry* 2012;72:595–603. doi:10.1016/j.biopsych.2012.04.028.
- [9] Jenkinson M, Beckmann CF, Behrens TE, Woolrich MW, Smith SM. FSL. *Neuroimage* 2012;62:782–90. doi:10.1016/j.neuroimage.2011.09.015.
- [10] Bullmore ET, Suckling J, Overmeyer S, Rabe-Hesketh S, Taylor E, Brammer MJ. Global, voxel, and cluster tests, by theory and permutation, for a difference between two groups of structural MR images of the brain. *IEEE Trans Med Imaging* 1999;18:32–42.
- [11] Awiszus F. Fast estimation of transcranial magnetic stimulation motor threshold: is it safe? *Brain Stimul* 2011;4:53–8. doi:10.1016/j.brs.2010.09.004.
- [12] Mir-Moghtadaei A, Caballero R, Fried P, Fox MD, Lee K, Giacobbe P, et al. Concordance Between BeamF3 and MRI-neuronavigated Target Sites for Repetitive Transcranial Magnetic Stimulation of the Left Dorsolateral Prefrontal Cortex. *Brain Stimul* 2015;8:965–73. doi:10.1016/j.brs.2015.05.008.
- [13] Fox MD, Liu H, Pascual-Leone A. Identification of reproducible individualized targets for treatment of depression with TMS based on intrinsic connectivity. *Neuroimage* 2013;66:151–60. doi:10.1016/j.neuroimage.2012.10.082.
- [14] Yeo BT, Krienen FM, Sepulcre J, Sabuncu MR, Lashkari D, Hollinshead M, et al. The organization of the human cerebral cortex estimated by intrinsic functional connectivity. *J Neurophysiol* 2011;106:1125–65. doi:10.1152/jn.00338.2011.
- [15] Lacadie CM, Fulbright RK, Rajeevan N, Constable RT, Papademetris X. More accurate Talairach coordinates for neuroimaging using non-linear registration. *Neuroimage* 2008;42:717–25. doi:10.1016/j.neuroimage.2008.04.240.